The α-helical regions of KERP1 are important in Entamoeba histolytica adherence to human cells

Doranda Perdomo, Bruno Baron, Arturo Rojo-Domínguez, Bertrand Raynal, Patrick England, Nancy Guillén

SCIENTIFIC REPORTS

OPEN

The α-helical regions of KERP1 are important in *Entamoeba histolytica* adherence to human cells

Doranda Perdomo[1,2,3], Bruno Baron[4,5], Arturo Rojo-Domínguez[6], Bertrand Raynal[4,5], Patrick England[4,5] & Nancy Guillén[1,2]

[1]Institut Pasteur, Cell Biology of Parasitism Unit, F-75015 Paris, France, [2]INSERM U786, F-75015 Paris, France, [3]Université Paris Diderot, Sorbonne Paris Cité, Cellule Pasteur, rue du Docteur Roux, F-75015 Paris, France, [4]Institut Pasteur, Plate-Forme de Biophysique des Macromolécules, F-75015 Paris, France, [5]CNRS UMR3528, F-75015 Paris, France, [6]Universidad Autónoma Metropolitana. Unidad Cuajimalpa. Departamento de Ciencias Naturales. Pedro Antonio de los Santos 84, 11850 México, D.F. México.

The lysine and glutamic acid rich protein KERP1 is a unique surface adhesion factor associated with virulence in the human pathogen *Entamoeba histolytica*. Both the function and structure of this protein remain unknown to this date. Here, we used circular dichroism, analytical ultracentrifugation and bioinformatics modeling to characterize the structure of KERP1. Our findings revealed that it is an α-helical rich protein organized as a trimer, endowed with a very high thermal stability (Tm = 89.6°C). Bioinformatics sequence analyses and 3D-structural modeling indicates that KERP1 central segments could account for protein trimerization. Relevantly, expressing the central region of KERP1 in living parasites, impair their capacity to adhere to human cells. Our observations suggest a link between the inhibitory effect of the isolated central region and the structural features of KERP1.

I n this study we focus on *Entamoeba histolytica*, the etiological agent of amoebiasis, an infectious disease targeting the intestine and the liver of humans[1]. To understand how the infectious process occurs, we directed our research towards KERP1, an important factor associated with the virulence of *E. histolytica* that has no homology to other known protein. This unique protein contains 25% lysine and 19% glutamic acid residues, and was first identified through its interaction with the brush border of human enterocytes[2]. Recent studies showed that *kerp1* gene expression is upregulated in virulent trophozoites and remarkably, downregulation of *kerp1* gene expression abolishes the capacity to form liver abscesses in the animal model[3]. The high number of charged residues in KERP1 suggests that it could have a propensity to form α-helical structures and that these helices may fold into coiled coils (CC). This motif commonly consists of two to seven α-helices, composed of $(a-b-c-d-e-f-g)_n$ heptad amino acid repeats[4]. About 70–75% of the **a** and **d** positions are occupied by apolar hydrophobic residues and positions **e** and **g** by polar hydrophilic residues mostly exposed to the solvent. This amino acid pattern favors the formation of α-helices that can oligomerize in a diverse range of fibrillar structures, commonly organized as dimers or trimers[5,6]. CC motifs are found in all proteomes, representing 4.3% in humans, 3.1% in bacteria and 1.9% in Archaea[7]. These motifs are well represented in proteins playing a significant role in the crosstalk of microbes with their host cells, as evidenced by the CC proteins participating in the Type III secretion system of pathogenic bacteria[8,9]. They are either involved in a single specific function or have multiple roles, as in the case of the Universal Stress Protein A (UspA), which acts as a host adherence molecule and mediates bacterial resistance to serum[10,11], pathogen survival in low pH conditions, oxidative stress or phagocytosis by the host[12]. Membrane fractions of *E. histolytica* are enriched in KERP1[2], however to date there are no studies linking KERP1 structure with its mode of involvement in the infectious process. Here we report different molecular-scale biophysical studies aiming to characterize the structure and function of KERP1. Circular dichroism (CD) allowed the analysis of the secondary structure and the thermal stability, while analytical ultracentrifugation (AUC) provided insight into the oligomeric architecture of the protein. Overall, our results show that KERP1 is an α-helical trimer that is able to reversibly unfold during thermal denaturation with a thermal melting point (Tm) of 89.6°C, never seen before for an *E. histolytica* protein. Bioinformatics analyses predicted three CC regions within KERP1 central segment and tertiary structure modeling suggested that one of these regions play a central role in trimer
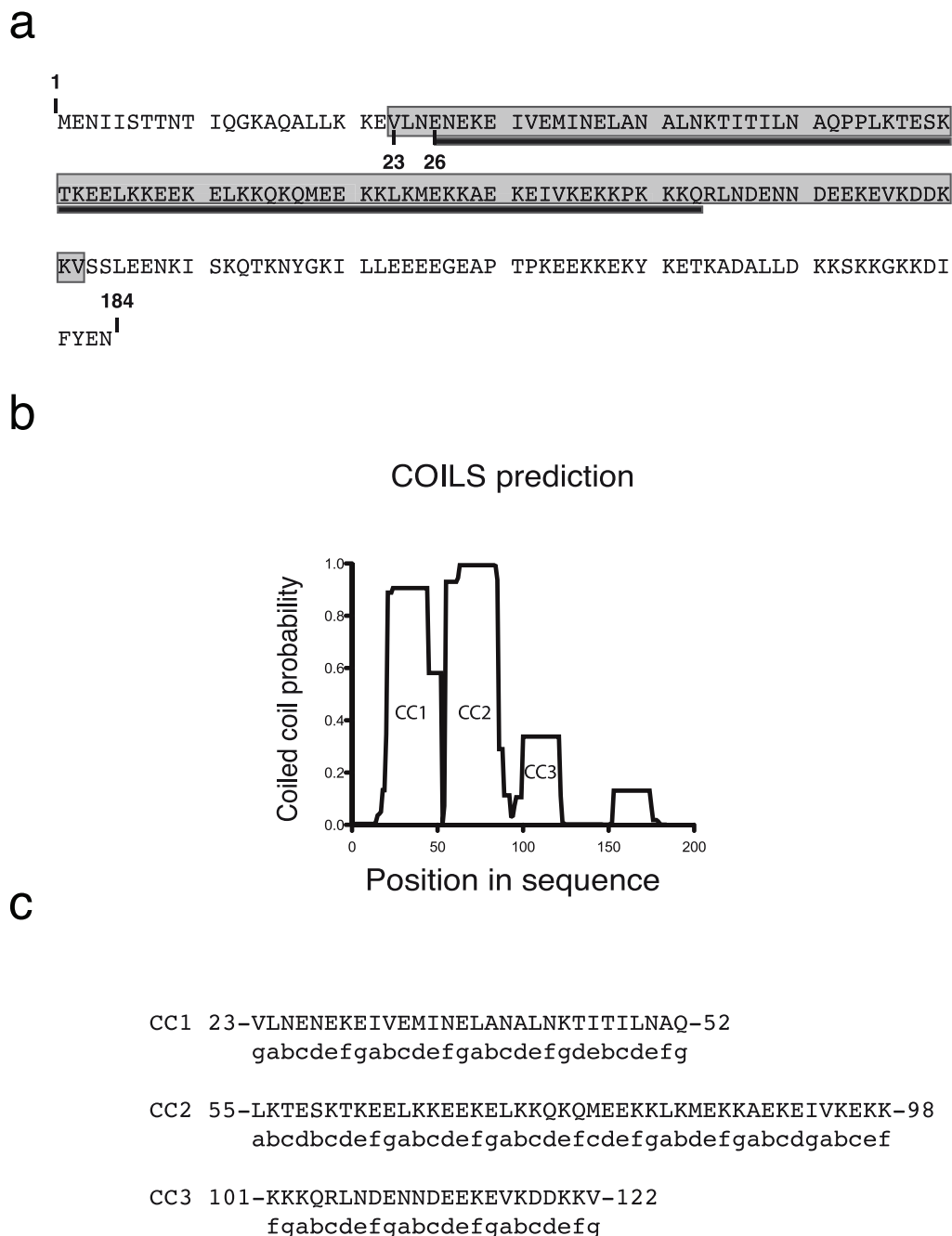
formation. Interestingly, expression of the KERP1 CC domains in living parasites reduced the parasite adhesion to human cells.

Results

Bioinformatics analysis of KERP1. As no KERP1 homologue could be found in any known proteome, we performed a bioinformatics analysis of its amino acid sequence to identify potential functional and structural domains present in this protein. To this end we used diverse secondary structure prediction software, and clearly obtained a statistical significant structural prediction with COILS. The COILS software[13] takes into account potential discontinuities in the periodically recurrent heptad because naturally occurring coiled-coils are often not homogeneous throughout their entire structure but rather interrupted by amino acids that alter the heptad repeat. Our scanning was set with parameters of 21-window size, an MTK matrix and a weighting option specifically designed for proteins with charged residues[14]. We thus found that amino acids 23 to 122 of KERP1 (Figure 1a) are predicted to fold into α-helices and have a high probability to adopt CC arrangements (Figure 1b and 1c, Supplemental Table 1) with leucine very often in position **a** of the heptad. Three regions with high coiled-coil folding propensity were identified: CC1 (residues 23 to 52), CC2 (residues 55 to 98) and CC3 (residues 101 to 122); from now on will be referred as KERP1 central segment (KCS). CC2 domain presenting stammers or stutters within the heptades.

a

```
1
|
MENIISTTNT IQGKAQALLK KEVLNENEKE IVEMINELAN ALNKTITILN AQPPLKTESK
                          23  26
TKEELKKEEK ELKKQKQMEE KKLKMEKKAE KEIVKEKKPK KKQRLNDENN DEEKEVKDDK

KVSSLEENKI SKQTKNYGKI LLEEEEGEAP TPKEEKKEKY KETKADALLD KKSKKGKKDI
       184
FYEN|
```

b

COILS prediction

c

```
CC1 23–VLNENEKEIVEMINELANALNKTITILNAQ–52
       gabcdefgabcdefgabcdefgdebcdefg

CC2 55–LKTESKTKEELKKEEKELKKQKQMEEKKLKMEKKAEKEIVKEKK–98
       abcdbcdefgabcdefgabcdefcdefgabdefgabcdgabcef

CC3 101–KKKQRLNDENNDEEKEVKDDKKV–122
        fgabcdefgabcdefgabcdefg
```

Figure 1 | KERP1 protein domains predicted by bioinformatics analysis. (a). Analysis of KERP1 primary structure using the COILS and Pfam servers. The coiled-coil domain (KCS) is highlighted in grey (from amino acid 23 to 122) and the Universal Stress Protein (Usp) domain (amino acid 26 to 103) is underlined in black. (b). Graphical representation of the COILS server prediction output using the complete amino acid sequence of KERP1 (Accession number EHI_098210). (c). Coiled-coil domain segments of KERP1 CC1 (residues 23 to 52), CC2 (residues 55 to 98) and CC3 (residues 101 to 122) are represented using the heptad repeat (a-b-c-d-e-f-g)$_n$ assignation from COILS prediction.

Although further search in the Protein family database Pfam also suggested the presence of a domain sharing homology with the UspA pathogenic factor, within KCS, spanning from residue 26 to 103 (Figure 1a) with an E value of 5.60e-03. These features prompted us to focus more precisely on KCS, to understand its role in live trophozoites and to gain insight about its structural features within KERP1.

Expression of KERP1 central segment in trophozoites reduces their adhesion to human cells monolayers. To examine the relevance of KCS in the function of KERP1 *in vivo*, we introduced the corresponding DNA into an expression plasmid suitable for amoeba, under the control of a tetracycline (Tet) inducible promoter. The rationale is that a peptide with CC propensity such as KCS could perturb the functions of its parent protein KERP1. We have previously used a similar strategy to demonstrate the negative effect of a coiled-coil region from the myosin II heavy chain on the activity of the endogenous protein, where it showed a direct effect in parasite motility and cell division[15]. Inducible KCS expression was investigated (after tetracycline induction) by immunoblotting the protein extracts from parasites transfected with either the control plasmid (TetOCat) or the plasmid carrying the KCS-encoding DNA (TetOCat KCS). Specific antibodies directed against endogenous KERP1 (anti-KERP1) or recombinant protein (anti-HSVtag) identified a protein with a molecular mass of 22 kDa, corresponding to KERP1, in all samples. KCS (15 kDa) was only detected in extracts from TetOCat-KCS amoebas induced with Tet for 48 hours (Figure 2a). We then decided to localize KCS in live parasites, employing immunofluorescence and confocal microscopy analysis (Figure 2b). In parasites carrying the control plasmid, KERP1 was localized in the expected cellular compartments, e.g. the membrane and intracellular vesicles[2], with no background detection by the anti-HSVtag antibody. In trophozoites expressing KCS, the plasma membrane and intracytoplasmic vesicles were stained by both the anti-KERP1 and the anti-HSVtag antibodies, indicating the localization of KERP1 and KCS in the same subcellular compartments.

To analyze the potential dominant-negative phenotype of KCS on the known functions of KERP1, parasites expressing KCS were incubated with human enterocytic (Caco2 line) or liver sinusoidal endothelial (LSEC line) cell monolayers. Previous work has shown the ability of *E. histolytica* to adhere and kill LSEC[16,17] and Caco2 cells[2,18]. For adherence assays, trophozoites were left to interact with the host cells for 30 minutes, allowing parasite adhesion with a reduced destruction of the monolayer. Contrary to currently used assays[19,20] in which the human cell monolayer is fixed with formaldehyde prior to incubation with parasites; our experiments keep both the host cells and the trophozoites alive. This procedure has the advantage of preserving the accessibility of potential surface receptors that could recognize *E. histolytica*. The experiments showed that KCS expression resulted in a significant reduction of trophozoite adherence to both types of mammalian cells (Figure 3a and 3b), with 50% less adherence in the case of LSEC and 60% less for Caco2 cells, when compared to parasites transfected with the control plasmid (n=3; p=0.004 for LSEC and p=0.002 for Caco2). A similar reduction was not observed in cytotoxicity assays, as incubation with both TetOCat and TetOCat-KCS transfected parasites induced equivalent host cell damage after one hour of incubation (Figure 3c and 3d). Although the above described statistical analysis give confidence to values obtained for parasite adherence, we noticed a reduction for non-induced TetOCat-KCS parasites when incubated with Caco2 cells. At this point, we do not have a clear-cut explanation for this phenotype that we speculate could be the consequence of a leakage expression from the plasmid, phenomenon already described[21]. The amount of protein leakage, although unperceivable in the western blot might lead to a distinct effect on parasite adherence on Caco2 cells whose surface is different to those of LSEC. Interestingly,

localization of KCS in live parasites upon interaction with human cells, employing immunofluorescence and confocal microscopy analysis showed the protein in the same cellular compartments as KERP1, the plasma membrane and intracytoplasmic vesicles (Supplemental Figure 2), as expected.

KERP1 is an α-helical structured and highly stable protein. In order to elucidate the major structural features of KERP1 and KCS we first employed molecular-scale biophysical approaches. The genes encoding KERP1 and KCS were cloned, expressed and the proteins purified from *Escherichia coli*, separately. Dynamic light scattering (DLS) measurements (data not shown) demonstrated that both KERP1 and KCS preparations obtained were homogenous (15% polydispersity) and free from protein aggregates.

Circular dichroism (CD) spectra in the far-UV region were recorded for both proteins (Figure 4a). The KERP1 CD profile exhibited two negative dichroic minima at 222 nm and 208 nm and a positive dichroic band with a maximum at 192 nm characteristic of a protein with high α-helix content. Deconvolution of the spectra, using a large reference dataset as specified in materials and methods, allowed to determine that 40% of KERP1 was folded in α-helices, 10% in ß-turns and 17% in turns while 29% was unordered (NMRSD of 0.01). If, more simply, a $\Delta\varepsilon$ (222 nm) of 12.1 $M^{-1}.cm^{-1}$ (ellipticity of 40000 $deg.cm^2.dmol^{-1}$) is assumed for 100% helicity, an α-helix content of 33% would be estimated for KERP1. As for KCS, it exhibited two negative dichroic bands at 222 nm and 205 nm, indicating a simultaneous presence of α-helices (30%, according to the calculation based on 222 nm ellipticity) and a high proportion of structural disorder.

The far-UV spectra of KERP1 (and KCS) revealed a ratio between the 222 nm and 208 nm signals that was lower than 1, contrary to what is expected for canonical coiled coil proteins (ratio >1)[22]. Nevertheless proteins with high index of α-helices can form coiled coil segments with 222/208 ratios <1, as observed for the PV "Velcro peptide" model[23].

We further employed CD to evaluate the thermostability of both proteins by following the loss of the CD signal (ellipticity) at 222 nm (dichroic band characteristic for α-helical proteins) when increasing the temperature of the sample from 10 to 100°C. KERP1 demonstrated a sigmoidal thermal denaturation profile, reflecting cooperative protein unfolding. The Tm was calculated at 89.6°C according to a two-state model (Figure 4b). On the contrary, KCS unfolded between 10°C and 60°C without a cooperative transition (Figure 4b), a behavior characteristic of proteins with high proportions of unstructured regions. These results suggest that the amino and/or carboxyl termini of KERP1 (absent in KCS) are necessary for the correct folding of the protein and its high thermal stability. Interestingly, the denaturation of KERP1 was almost completely reversible, as demonstrated by renaturing the sample from 100° to 10°C, under the same experimental conditions, and observing that the loss in ellipticity was only of 5% (Figure 4c).

KERP1 oligomerizes as an elongated trimer. To further investigate the size, shape and oligomeric organization of KERP1 we performed analytical ultracentrifugation (AUC) using sedimentation velocity. KERP1 was present as a single species over a wide concentration protein range with a sedimentation coefficient ($S_{20,w}$) of 2.8S and a frictional ratio (f/f_0) of 2.0 corresponding to a molecular mass of 65.6 kDa (Figure 5a and 5b). These values suggest that KERP1 is organized as a trimer with a rod like shape as observed for other α-helical rich proteins[24]. As for KCS, it displayed characteristics of a protein undergoing homo-association equilibrium. After testing different self-association models, we found that only a monomer/trimer model could fit correctly our data. The sedimentation coefficients (S_{20w}) of the monomer and the trimer were respectively 1.8S and 4.3S with an estimated dissociation equilibrium constant (Kd) of 3.8×10^{-9} M^2. We calculated a frictional ratio of 1.1 for both the

a

b
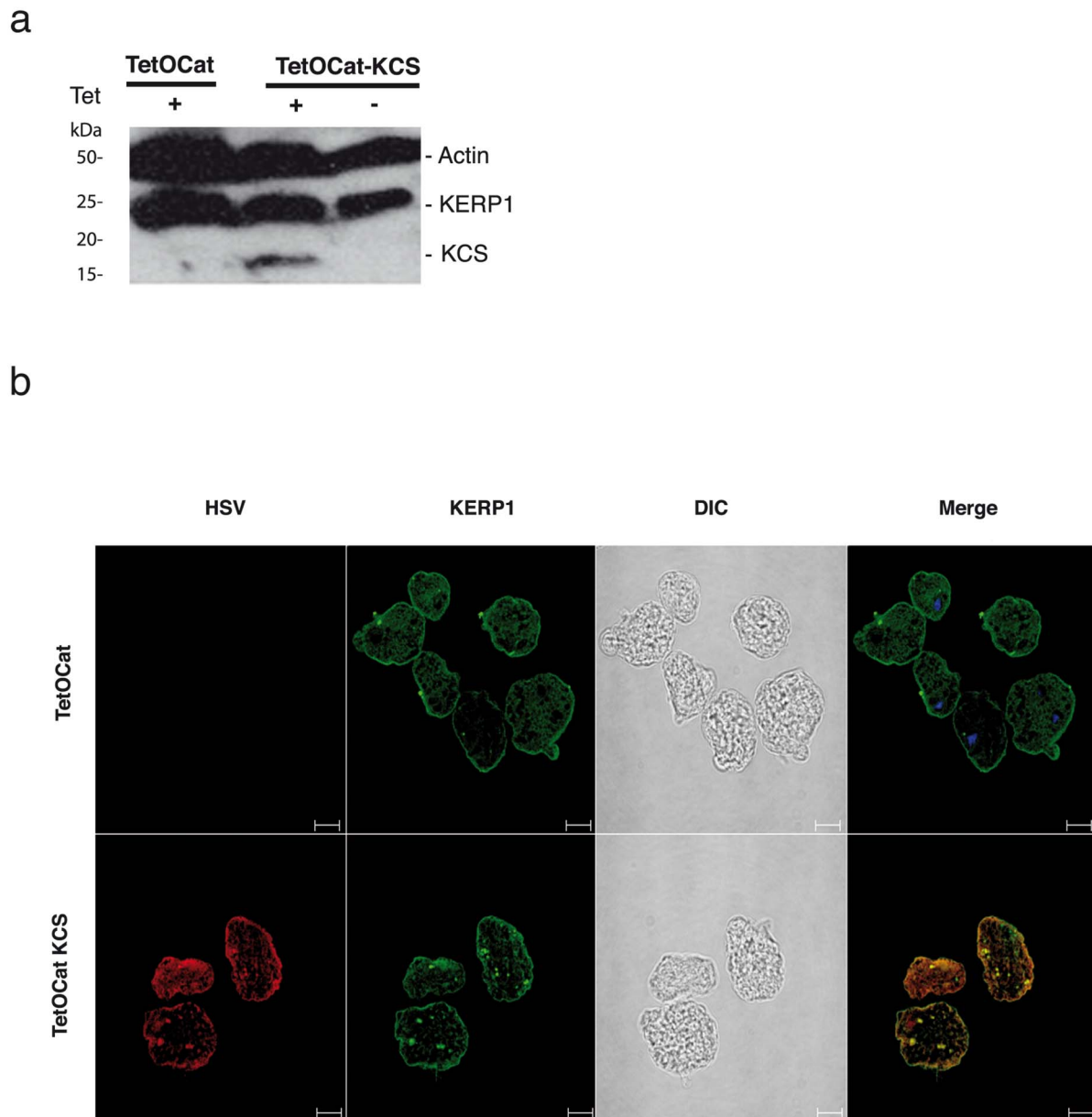
Figure 2 | KCS is expressed in *E. histolytica* transfectants and localizes in the same cellular compartments as KERP1. Biochemical detection of KERP1 and KCS in transfected trophozoites TetOCat and TetOCat-KCS. (a). Immunoblotting of parasite protein extracts at 48 hours of tetracycline induction (+) or without (−). Detection of endogenous actin (49 kDa; mAb anti-actin C4) was used as protein extract loading control. Detection of KERP1 (25 kDa; mAb anti-KERP1 C2-7) in all strains was observed, but detection of HSV-KCS (15 kDa; mAb anti-HSVtag) was only remarked in TetOCat-KCS (+). Immunoblotting was performed using simultaneously all the primary antibodies. (b). Endogenous KERP1 colocalizes with KCS in live parasites. Cellular detection of KERP1 and KCS in transfected trophozoites TetOCat and TetOCat-KCS after 48 hours of tetracycline induction. Micrographs showing immunofluorescence images acquired by confocal microscopy. KERP1 is detected by a specific monoclonal antibody (green; mAb C2-7), KCS by the HSV-tag (red; mAb anti-HSVtag) and nuclei are labeled with DAPI (blue). KERP1 and KCS share the same cellular compartment as observed by the concentrated patches (yellow) at the trophozoite plasma membrane and internal vesicles. Focal planes from a Z-stack were selected. Scale bar 10 μm.

monomer and the trimer, which is indicative of a globular shape (Figure 5c and 5d). Thus, although KCS alone has the ability to oligomerize, the amino and/or carboxyl termini of KERP1 are necessary to stabilize the trimeric assembly of the full-length protein.

Overall the biophysical structural characterization we performed portrays KERP1 as a highly thermostable α-helical rich and elongated trimeric protein, compatible with the presence of CC domains. Regions outside KCS (at the amino and/or carboxyl termini of KERP1) are required to correctly fold and oligomerize the protein.

Structural modeling of KERP1. Crystallization trials were undertaken with purified KERP1 in order to determine its atomic-scale structure; however we failed to obtain crystals, even at high concentrations of KERP1 (60 mg.ml^{-1}). Nonetheless, to obtain 3D-structural information, we recurred to bioinformatics modeling of KERP1 using the LOMETS threading software[25]. LOMETS regroups eight prediction servers to estimate a possible structure of a protein that lacks homologues. Among the different possible monomer models proposed for KERP1, we highlighted the top ranked model with a Zscore = 5.62. The 3D- structure was inferred by LOMETS by
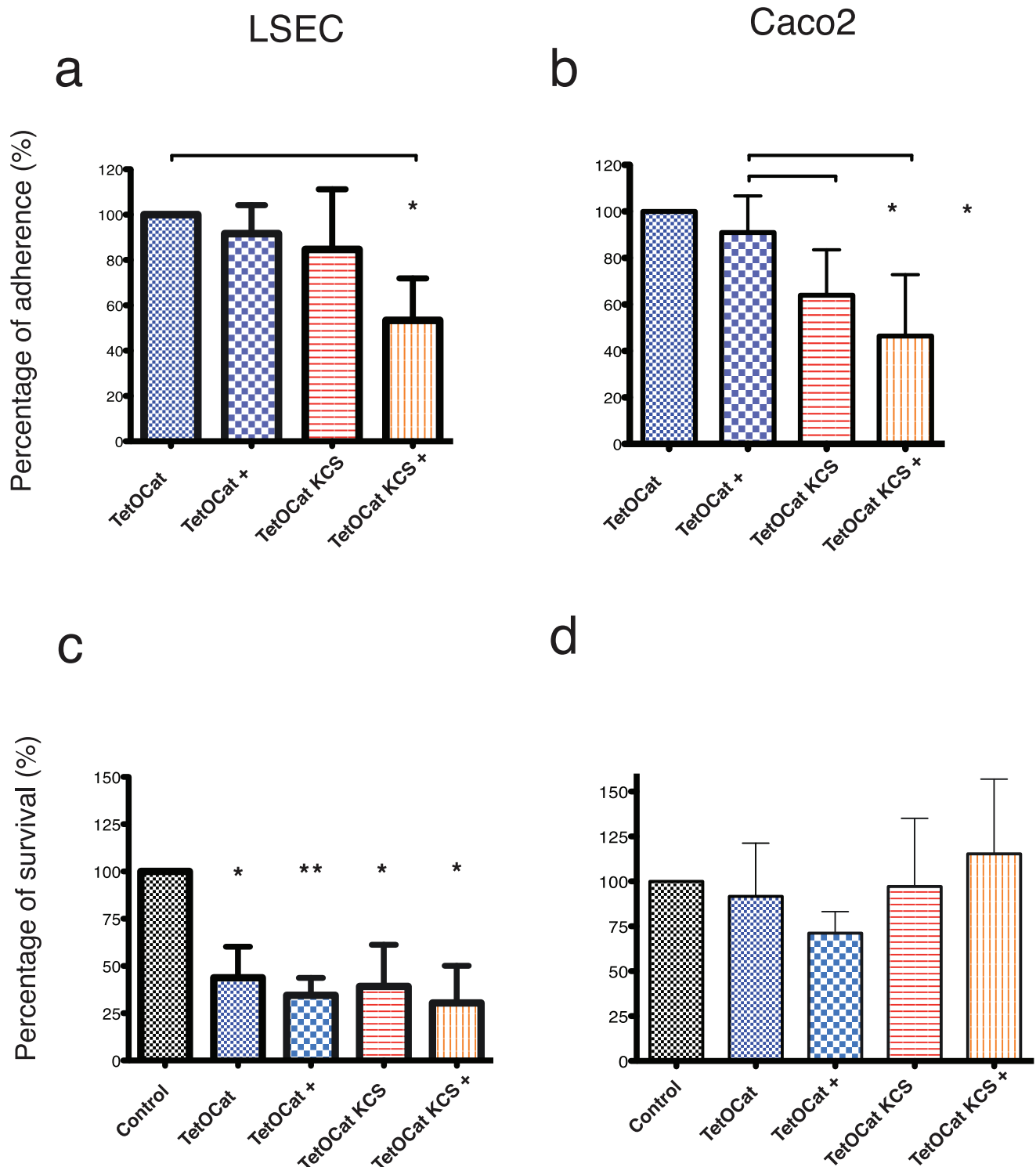
Figure 3 | Expression of KERP1 coiled-coil domains in *E. histolytica* reduces the capacity to adhere to human cells without affecting cytotoxicity. Functional assays of adherence and cytotoxicity using *E. histolytica* transfectants TetOCat and TeTOCat-KCS with (+) or without (−) induction by tetracycline, interacting with human cells LSEC or Caco2. Assays were performed in a ratio of 1:5 amoebas to human Caco2 cells and 1:10 to human LSEC. (a). Percentage values of adherence to LSEC (p value: 0.004). (b). Percentage values of adherence to Caco2 cells (p value: 0.002). A statistically significant reduction of 60% in adherence is observed for trophozoites expressing KCS (TetOCat-KCS+) compared to the control (TetOCat), independently of the human cell type. Cytotoxicity assays were performed using the same ratio as before with a control sample without parasites, indicating the 100% rate of survival of the human cells during the experiment. (c). Percentage values of LSEC survival (p value *: 0.02; **: 0.006). (d). Percentage values of Caco2 cell survival. No difference in the percentage of survival between the different human cell lines was observed upon comparison with the control.

a

b

c
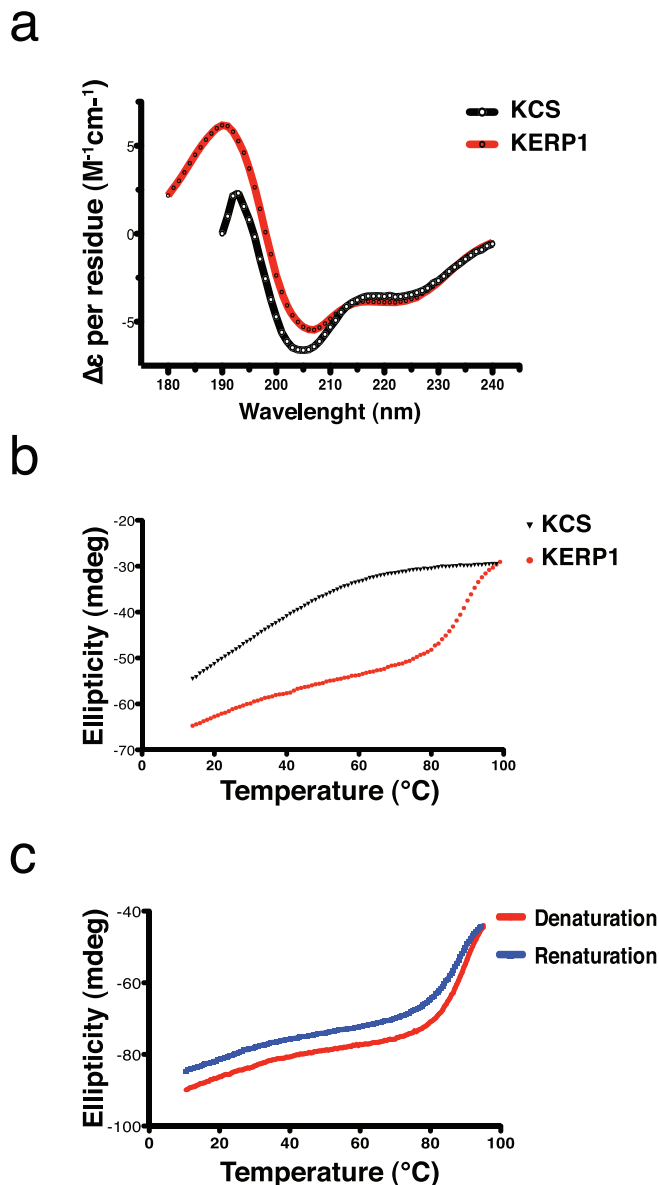
Figure 4 | KERP1 is an α-helical protein highly stable to thermal denaturation. (a). KERP1 and KCS secondary structure analysis determined by following circular dichroism signal in the far–UV region. KERP1 shows two negative peaks minima at 222 nm and 208 nm that highlight the content of α-helices in the protein (red) contrary to KCS with two negative peaks minima at 222 nm and 205 nm that highlight the content of unstructured regions in the protein (black). (b). Thermal denaturation of KERP1 was observed by the loss in ellipticity at 222 nm when increasing temperature (10° to 100°C). The thermal melting point was calculated using a two-state cooperative transition obtaining a value of 89.6°C for KERP1 (red) and 60°C for KCS (black). (c). Melting curves for KERP1, measured by monitoring the absorbance at 222 nm against increasing (denaturation) and decreasing temperatures (renaturation).

homology with the C-terminal fragment of tropomyosin (PDB accession number 2EFR chain A) a protein highly rich in α-helices. The model for KERP1 displayed an elongated α-helix (Supplemental Figure 1a and b and Supplemental Table 2), with most of the lysine (K) residues exposed to the protein surface. This threading monomer model appears to be compatible with the rod-like shape of KERP1 trimer determined from the AUC values (frictional ratio); nevertheless the computer prediction does not fully correspond with the secondary structure content of KERP1 deduced from the CD analysis.

KERP1 single trimeric species

KCS monomer trimer equilibrium
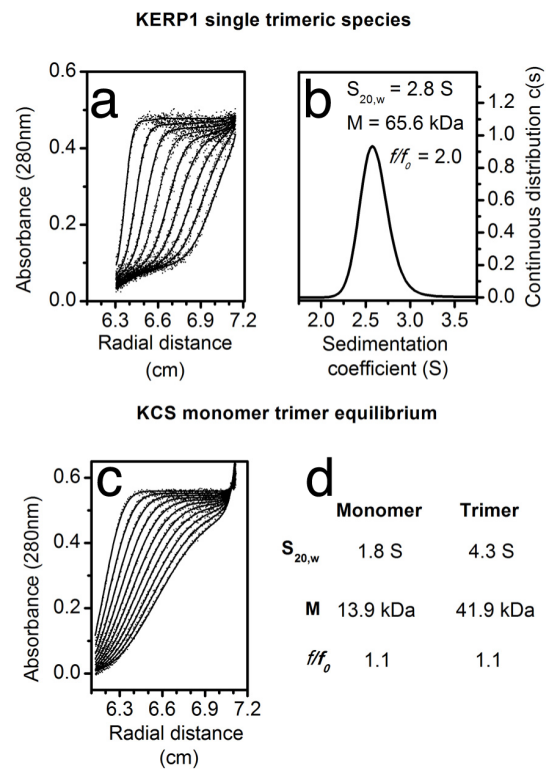
Figure 5 | Analytical ultracentrifugation characterization of KERP1 and KCS. Sedimentation velocity analysis of KERP1 (a and b) and KCS (c and d) at 20 μM. (a) Radial distribution of optical density measurements at 280 nm of KERP1: experimental data (dot), and fitted line (RMSD <0.006) to the continuous distribution model. (b) Sedimentation coefficient distribution c(s) showing a single peak compatible with a trimeric form of KERP1 with its hydrodynamic properties. (c) Radial distribution of optical density measurements at 280 nm of KCS experimental data (dot), and fitted line (RMSD <0.005) to the self-association monomer/trimer model. (d) Hydrodynamic properties of KCS monomer and trimer.

Then the three regions of KERP1 potentially organized in coiled-coils according to COILS software (CC1, CC2 and CC3) were independently examined to determine their probability of being involved in KERP1 trimerization, by performing molecular dynamics simulations using MOE (Molecular Operating Environment, www.chem-comp.com; Supplemental pdb files 1, 2 and 3). Calculations were performed based on free energy binding and the structure of a human kinase (PDB ID 1WT6) as a template, which was selected based on its trimeric coiled-coil oligomerization, comparable to that predicted for KERP1. Considering the electrostatic environment within the CC regions, we calculated their cooperativity, e.g. the difference between the electrostatic energy of the trimer and the sum of the electrostatic energies for independent monomers. These calculations resulted in cooperativity values (Figure 6) of -78, -4 and -594 kcal.mol^{-1} respectively for CC1, CC2 and CC3. In the case of KCS, CC1 and CC3 include extra electric charges at their amino and carboxyl termini, respectively. Recalculation of cooperativity due to this difference yielded changes of around 20 kcal.mol^{-1}, not significant for discussion. From these results, we suggest that CC3 is the protein fragment with the highest trimerization propensity, as judged by electrostatic analysis of the model. The fragments CC2 or CC1 in contrast present weaker interaction, indicating that indeed these have lower probability to start the trimerization. Furthermore a structural exploration of interchain contacts in the CC3 trimer shows a clear system of alternate positive and negative electric charges between Glu112, Glu115 and Asp119 of one helix intercalated with
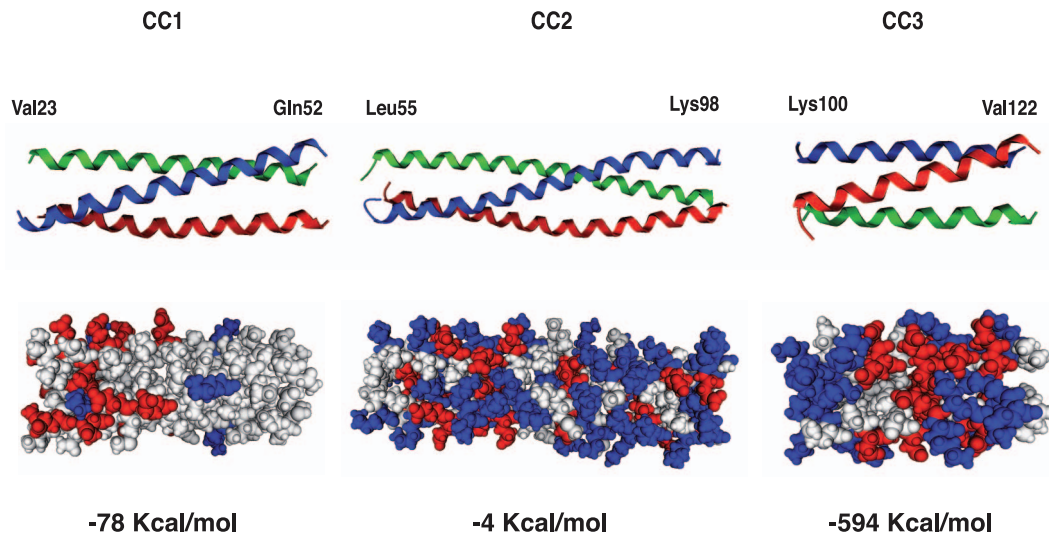
Figure 6 | Three-dimensional structure prediction of KERP1 trimeric coiled-coil regions. Three-dimensional modeling of the CC regions predicted for KERP1 according to COILS results. CC regions of KERP1 correspond to the KCS protein designated as, CC1 (Valine23 to Glutamine52), CC2 (Leucine55 to Lysine98) and CC3 (Lysine100 to Valine122), folded as elongated trimer. Modeling was performed using chain A of PDB file ID 1WT6 as template with its distinctive trimeric coiled-coil organization. Each of the three alpha helical ribbon chains is colored differently in order to differentiate them. Under the ribbons CPK model highlight the presence of positively charged residues (blue) and negatively charged residues (red). The most stable coiled coil trimer corresponds to CC3 (residues Lys-100 to Val-122) according to an electrostatic analysis on each of the CC predicted regions and the calculated values of free energy present for each, represented in the bottom of the CPK models.

Lys117 and Lys120 of the other. Charge deactivation in any of these residues yields strong destabilization of chain-chain interaction in the trimer, being Glu 115 and Lys117 the strongest contributors with around 300 kcal.mol^{-1} each.

Discussion

In previous work the importance of KERP1 in pathogenesis has been highlighted by (i) its association to host cells surfaces such as the brush border of human enterocytes, (ii) its high expression level in virulent parasites and (iii) its importance in the development of liver abscesses in the hamster animal model[2,3]. However, the specific function of KERP1 remains to be identified. To this end, we decided to explore *E. histolytica* parasite complex interactions with human cells, which include (i) adherence[19], (ii) cytotoxicity[19,20,26] and (iii) phagocytosis[26,27]. To gain insight into KERP1 role, we took advantage of the fact that its central segment (KCS) was predicted to be a coiled coil, and assumed that its expression could interfere with endogenous KERP1 (alone or as a partner in a specific interactome) and originate phenotypical changes in the parasite.

We showed that KERP1 and KCS localized in the same subcellular compartments, including vesicular patches within the cytoplasm and the cell surface, whether the trophozoites were alone or incubated with human cells. The expression of KCS in trophozoites did not induce significant morphological differences compared to control parasites indicating that the protein *per se* is not toxic. We noticed that KCS had a clear impact on parasite adhesion to epithelial and endothelial cells. The phenotype linked to this effect could be explained by two different mechanisms: (i) the expression of KCS may destabilize the trimeric structure of KERP1 by electrostatic effects resulting in an inactive state of KERP1 (ii) KCS could compete with KERP1 for binding to cellular partners important for its function and that remain to be identified. Considering that KERP1 has an Usp domain, predicted within KCS, it may account for important pathogenicity-linked functions. Usp domains are known in bacteria such as *Moxarella catarrhalis*[10], for their involvement in adherence; as well as, in oxidative stress defense, iron homeostasis and motility/cell adhesion in *Listeria monocytogenes*[12]. Changes in the expression levels of Usp domain-containing proteins correlate with

modulations in displayed virulence[28]. In the case of *E. histolytica*, increased virulence correlates with high levels of KERP1[3]. However, the expression of Usp domain-containing KCS did not significantly change the cytotoxicity (Figure 3) or RBC phagocytosis (data not shown), indicating that reduced parasite adherence is not correlated to cell damage. These observations are comparable to those obtained with trophozoites blocked for Gal/GalNAc lectin functions, in which a reduction in adherence to enterocytes was observed, while maintaining high levels of cytotoxicity[29,30]. Residual parasite adhesion in KCS or Gal/GalNAc engineered parasites should account for the high cytotoxicity levels.

To better understand the basis of KERP1 functional characteristics, we undertook the characterization of KERP1 structure. Using different bioinformatics and biophysical approaches, we showed that KERP1, possesses a trimeric α-helical rich core, possibly organized in coiled-coils, which is strongly stabilized by its amino- and carboxy-terminal regions. The global secondary structure is composed of a majority of α-helical structure, but also a significant amount of ß-sheets and unordered regions. Full length KERP1 is a tight elongated trimer with a high thermodynamical stability (Tm > 89°C), characteristic of oligomeric coiled-coil proteins, that reversibly unfolds according to a two-state cooperative transition. The impressive thermodynamic stability of KERP1 could be explained by its high lysine and glutamic acid content that allow an electrostatic charge complementarity in a similar fashion to that used to stabilize the heterodimeric designed ACID-BASE PV model[23]. In PV, charged residues **e** and **g** create electrostatic interactions, while the hydrophobic **a** and **d** residues create van der Waals interactions, further stabilizing the heterodimer[23,31] which, as KERP1, displays a high thermal stability and unfolds reversibly. The main Velcro-like electrostatic interaction in KERP1 seems to be located in segment 112–120, being Glu 115 and Lys117 the major contributors, since computer vanishing of the charge of any of these residues reduced trimer stability to a half. Another possible explanation for KERP1 high thermostability could be provided by analogy with the right-handed tetrameric coiled-coil protein (RHCC) from the thermophilic organism *Staphylothermus marinus*. In RHCC, the abundant charged residues (27%) appear to form intra- and inter-helical salt bridges that create a favorable

network of hydrophobic and electrostatic interactions with a tetramer core filled of water, all characteristics contributing to a high Tm[32,4]. We can hypothesize that KERP1, as a virulence factor in *E. histolytica*, is stable in its host at temperatures above 40°C, specifically when a fever response is triggered during human immune response to amoebic infection, since its structure and possibly its function would be unaffected.

Analysis of KERP1 central segment, KCS, showed that it displayed a high degree of structural disorder, a non-sigmoidal thermal denaturation profile (characteristic of unstructured proteins) and a destabilized oligomerization interface, indicated by the presence of both monomers and trimers in solution (in concentration conditions in which KERP1 is purely trimeric). These results demonstrate that the KCS is not sufficient for the full stabilization of the fold and oligomeric assembly of KERP1, and that the amino- and/or carboxy-terminal parts of KERP1, absent in KCS, appear to play a significant contribution. Within KCS, modeling suggested that CC3, situated closest to the carboxy-terminus, played a preponderant role in stabilizing the trimer. Interestingly, CC2, the second and longest CC region, presents the highest number of charged residues, but electrostatic repulsions almost completely compensate the stabilizing charge pairs, thus suggesting it contributes only marginally to the stability of KERP1. Until now, no other virulence factor of *E. histolytica* has been reported with these structural characteristics of circular dichroism, unfolding reversibility and atomic-detail modeling.

Altogether, our study provides evidence for the involvement of KERP1 central segment in adherence to human cells, without any type of selectivity. These regions could potentially be folded in coiled-coils within KERP1, and could thus contribute to its high thermodynamic stability and trimeric architecture as reported for important microbial molecules participating in adherence to human cells. Overall we have gained significant insight into the function and structure of a virulence factor unique to *E. histolytica*.

Methods

Cell strains and culture. The axenic *E. histolytica* strain HM1:IMSS was cultured in TYIS-33 medium at 37°C[33]. Transfected parasites were maintained in culture with 10 μg ml⁻¹ hygromycin B. The human Colon carcinoma cell line TC7 (Caco2) and the human liver sinusoidal endothelial cell line (LSEC) were grown as previously described[2,16].

Cloning, transfection and expression of *kerp1* coiled-coil in *E. histolytica*. The KCS sequence was amplified from genomic DNA of HM1:IMSS strain using the following primers: 5′- ctggtaccatgagccagccagaactcgctcctgaagacccagaggatgtattaaatgaaaatgaa-aaagag-3′ adding a HSV tag to the protein N-terminus and 5′- gtggatccttaaa-ctttcttatcatcttttac-3′. The PCR product was cloned into the pCR2.1 TOPO plasmid (Invitrogen) according to the recommended protocol. The recombinant plasmid was purified and digested by *KpnI* and *BamHI*. The DNA fragment was ligated into pEhHYG-tetR-O-CAT vector[34] and thus cloned under the control of the Tet-inducible promoter. The plasmid was sequenced (Beckman Coulter Cogenics) to verify identity and orientation of the insert and transfected into HM1:IMSS virulent trophozoites as described[34]. Transfected strains, called kerp1central segment (KCS) and control plasmid without KCS, TetOCat, were maintained in culture with 10 μg ml⁻¹ hygromycin B. Prior to experiments, transfected strains were cultured with 10 μg ml⁻¹ hygromycin B for 24 h, then supplemented, or not, with 1 μg ml⁻¹ Tet for 48 hours.

Immunoblotting. Total *E. histolytica* crude protein extracts were obtained from 48 hours trophozoite cultures. Parasites were washed once in PBS and resuspended at 2 × 10⁶ parasites ml⁻¹ in 10 mM Tris pH 7.5, protease inhibitor mixture [Complete EDTA-free protease inhibitor cocktail, 10 mM leupeptin, 50 mM *N*-ethylmaleimide, 5 mM 4-Hydroxymercury benzoic acid sodium salt, PhosSTOP Phosphatase inhibitor cocktail, 10 μM E-64, 2 mM Na₃VO₄, 100 mM NaF, 10 mM Iodoacetamine] and lysed with 1% SDS at 100°C for 10 min. Protein samples corresponding to 2 × 10⁵ parasites were resolved by SDS-PAGE on a 20% acrylamide gel and electrotransfered onto a 0.2μm PVDF membrane. Proteins were detected by Western blotting using mouse anti-kerp1 monoclonal antibody (1 : 3000), mouse anti-actin monoclonal C4 antibody (1 : 10 000 dilution; MP Biomedicals), HSV tag mouse monoclonal antibody (1 : 3000; Novagene) and sheep peroxidase-conjugated anti-mouse IgG (1 : 10 000; G&E). Membranes were treated with ECL Western blotting detection reagent and exposed on Kodak Biomax film.

Immunofluorescence labelling of *E. histolytica* transfectants. Trophozoites were washed and resuspended in TYIS-33 medium with a density of 3 × 10⁵ cells ml⁻¹

spotted on a 22 mm² coverslip for 30 minutes at 37°C for adhesion. Trophozoites were fixed with 4% methanol-free formaldehyde for 30 minutes at 37°C, washed with 0.1 M glycine Dulbecco's phosphate buffer (DPBS), permeabilized with 0.5% Triton X-100 in PBS for 1 minute and finally 3% BSA-DPBS was added for 60 minutes. Samples were incubated with polyclonal anti KERP1 antibody (1 : 100), anti-HSV tag mAb (1 : 600; Novagene) followed by goat anti-rabbit Alexa Fluor 488 and goat anti-rabbit Alexa Fluor 546 (1 : 200; Molecular Probes both). Coverslips were mounted with ProLong antifading reagent containing DAPI (Molecular Probes). Images were acquired with an LSM700 confocal microscope (Zeiss). For immunofluorescence labeling of *E. histolytica* transfectants incubated with mammalian cell lines, parasites were washed and incubated to Caco2 and LSEC using the same conditions as for adherence experiments (see below). Cell fixation, labeling and mounting was performed as described.

Adherence assay. Human Caco2 cells were grown on 22 mm² coverslips until differentiation and LSEC grew on 22 mm round coverslips coated with fibronectin for 4 days. Adherence assays were carried out as described[35] with several modifications. Transfected parasites were labeled with 2.5 μM of orange-fluorescent tetramethylrhodamine cell tracker (CMTMR, C2927- Invitrogen) for 30 minutes in DPBS supplemented with 100 mg ml⁻¹ CaCl₂ and MgCl₂ at pH 7.4. Parasites were washed and resuspended in RPMI or DMEM, and added to the Caco2 or LSEC (2 × 10⁵ parasites per coverslip) for 30 minutes at 37°C under 10% or 5% CO₂. Coverslips were then washed twice with warm PBS, fixed with 4% formaldehyde for 30 minutes at 37°C, rinsed twice with PBS and mounted using ProLong antifading reagent (Invitrogen). Slides were scanned with LSM-700 confocal microscope for each transfected parasite cell line (supplemented or not with tetracycline) using five fields across the coverslip (objective 40X and 3 different slides). Data were expressed by calculating the percentage of adherence compared to the 100% control (TetOCat). Each condition was repeated three times on the same experiment and three independent experiments were performed for each cell line. Results were compared by a paired *t*-test.

Cytopathogenicity assay. Human Caco2 (differentiated) and LSEC cells were grown in 12-well plates as described above. Cells were rinsed twice in warm cell culture media and parasites were added to Caco2 1 : 5 and to LSEC in 1 : 10 ratio[16]. Control experiment was carried out without the addition of trophozoites. All conditions were incubated for 60 minutes at 37°C in 10% or 5% CO₂. Cells were washed twice with cold DPBS to detach the parasites and warm media was added to the human cells. Quantification of the survival rates for Caco2 and LSEC was performed using trypan blue coloration followed by cell counting in situ under the microscope. Data were expressed by calculating the percentage of survival compared to the 100% control. Each condition was repeated three times on the same plate and three independent experiments were performed. Results were compared by a paired *t*-test.

Cloning, expression and purification of recombinant KERP1 and KERP1-central segment in *Escherichia coli*. The KERP1 encoding gene (Accession number: EHI_098210) or the *kerp1* central segment region (KCS) was cloned into the inducible expression vector pET28 a+ (Novagene). First, the DNA was amplified by PCR from *E. histolytica* HMI-IMSS genomic DNA using the following primers for *kerp1*: 5′-gc catatggaaatattataagcacaacaaatac-3′ and 5′- gtctcgagttaattttcat-agaaaatatctttctttc-3′. For *kerp1* central segment: 5′- gtcatatggtattaaatgaaaatgaaaaagag -3′ and 5′-gt ctcgagttaaactttcttatcatcttttac-3′. PCR products were cloned into TOPO 2.1 Zero blunt vector and *Escherichia coli* strain H10F′ transformed and propagated in Luria Bertani (LB) media containing 50 μg ml⁻¹ Kanamycin. Recombinant plasmids were purified and digested by *NdeI* and *XhoI* restriction endonucleases, respectively. The digested fragments were ligated into pET28a+ expression vector, thus adding a 6-histidine tag at the 5′ of the inserted sequences. *E. coli* BL21 were transformed and propagated in 50 μg ml⁻¹ Kanamycin LB medium at 37°C. The recombinant plasmids were sequenced (Beckman Coulter Cogenics) to verify the sequence of *kerp1* and *kerp1* coiled-coil. Expression of recombinant proteins was induced with 1 mM isopropyl β-D-1-thiogalactopyranoside (IPTG) during 2 hours at 37°C under constant agitation. Proteins were purified in three-step procedure: First, bacteria were lysed in a French press in the presence of protease inhibitors (Roche) and Benzonase. The proteins were purified using the Ni-NTA Superflow purification kit for 6 histidine tag proteins (QIAGEN) following the manufacturer's protocol. An additional DNAse/RNAse (Ambion) digestion treatment was realized for the eluted samples, followed by a second passage through Ni-NTA Superflow columns. Secondly, the fraction containing the recombinant protein was passed through ion exchange column using a HiTrap SP HP (GE Healthcare) according to manufacturer's recommendation. The protein was finally purified by gel filtration chromatography, with a Superdex 200 column (GE Helthcare). KERP1 concentration was determined by measure of absorbance at 280 nm with the protein extinction coefficient of 4470 M⁻¹ cm⁻¹ (Abs₂₈₀ ₙₘ 1 g/L = 0.191). Protein quantification for KCS was done by amino acid analysis. Both proteins were kept at −80°C in 10 mM NaH₂PO₄, 300 mM NaCl pH 7.4 until further use.

Circular dichroism (CD). CD experiments in the far-UV region were performed using an Aviv CD spectrometer model 215 equipped with a water-cooled Peltier unit. KERP1 was concentrated at 0.8 mg ml⁻¹ and KCS at 0.5 mg ml⁻¹, both in 10 mM NaH₂PO₄ and 150 mM NaCl pH 7.4. The spectra were recorded in a cell width of 0.2-mm path length (121.QS, Hellma) from 180 to 260 nm for KERP1 and 190 to 260 nm for KCS (1 nm steps) at 25°C. Three consecutive scans from each sample were

merged to produce an averaged spectrum; the spectra were corrected using buffer baselines measured under the same conditions. Data were normalized to residue molar absorption measured in mdeg (M^{-1} cm^{-1}) and expressed as delta epsilon ($\Delta\varepsilon$). Secondary structure estimates were derived from the normalized spectra using the CDSSTR routine (Johnson, 1999) of the DICHROWEB server[36,37] run on the SP175[38] and base 1 datasets. Thermal denaturation of the proteins was measured by monitoring the change in ellipticity in a cell width of 0.1 cm path- length at 222 nm over the range of 10°C to 100°C, in increments of 1°C and expressed as delta epsilons ($\Delta\varepsilon$). Protein concentration was 0.5 mg ml^{-1} for KERP1 and KCS respectively, and buffer conditions were the same as above. In the case of denaturation/renaturation experiments, KERP1 was concentrated at 0.8 mg/ml in the same buffer conditions as before. The experimental denaturation profiles were analyzed by a nonlinear least squares fit assuming a two-state transition and used to calculate the melting temperature (T_m) and enthalpy of unfolding (ΔH)[39,40].

Analytical ultracentrifugation (AUC). Sedimentation velocity experiments were carried out in a ProteomeLab XL-I analytical ultracentrifuge (Beckman Coulter) equipped with double-UV and Rayleigh interference detection. Samples of KERP1 at 20 to 160 µM and samples of KCS at 20µM were prepared in 10 mM NaH2PO4, 150 mM NaCl pH 7.4, loaded in a 1.2 mm thick two-channel epon centerpiece and spun at 42 000 rpm at 20°C. Absorbance and interference profiles were recorded every 90 seconds. The density (1.01198 g ml^{-1}) and viscosity (0.01020 P) of the buffer as well as the partial specific volume of the proteins were estimated at 20°C by employing the Sednterp 1.09 software (http://www.jphilo.mailway.com/download.htm). Sedimentation coefficient distributions $c(s)$ were determined using the Sedfit 12.0 (http://www.analyticalultracentrifugation.com) software. In the case of KCS protein the homo-association was tested by global fitting with the software Sedphat 9.4 and the monomer-trimer model was used.

Molecular modeling. 3D models of KERP1 (NCBI accession number EHI_098210) were predicted at LOMETS servers (http://zhanglab.ccmb.med.umich.edu/LOMETS). LOMETS generates protein structure predictions by ranking and selecting models from 8 state-of-the-art threading programs. Molecular modelling and structural analysis of coiled-coil regions were performed with MOE (Molecular Operating Environment, www.chemcomp.com) with CHARMM27 force field. Structural modelling of KERP1 segments were based on the chain A of the PDB file ID 1WT6 (Coiled-coil domain of myotonic dystrophy protein kinase) with a sequence alignment directed by the adjustment of hydrophobic amino acids in the residue heptads. The modelling procedure included generation of 50 structures differing only in the conformation of their side chains, followed by energy minimization until a gradient of 0.1 kcal/(mol Å) was reached. Among them, the lowest energy structure was selected as the final model, which in turn was further optimized until a gradient of 0.05 kcal/(mol Å) was achieved. The segment 22 to 123 of KERP1, called central segment (KCS), was parsed by the positions of proline and glycine residues into three coiled-coil regions: 23–52, 55–98 and 100–122. Electric charges at amino and carboxyl termini of each modelled segment of KERP 1 were pasivated by acetylation or amination, respectively; except for residues 23 and 122 in the case of KCS, since these are real amino and carboxyl termini for the protein segment. The cooperativity or energy of monomer-trimer interaction was calculated by subtracting in each CC region the sum of electrostatic energies of isolated monomers to the energy of the trimer.

1. Stanley, S. L. Jr. Amoebiasis. *Lancet* **361**, 1025–1034 (2003).
2. Seigneur, M., Mounier, J., Prevost, M. C. & Guillen, N. A lysine- and glutamic acid-rich protein, KERP1, from Entamoeba histolytica binds to human enterocytes. *Cell Microbiol* **7**, 569–579 (2005).
3. Santi-Rocca, J. *et al.* The lysine- and glutamic acid-rich protein KERP1 plays a role in Entamoeba histolytica liver abscess pathogenesis. *Cell Microbiol* **10**, 202–217 (2008).
4. Burkhard, P., Stetefeld, J. & Strelkov, S. V. Coiled coils: a highly versatile protein folding motif. *Trends Cell Biol* **11**, 82–88 (2001).
5. Parry, D. A., Fraser, R. D. & Squire, J. M. Fifty years of coiled-coils and alpha-helical bundles: a close relationship between sequence and structure. *J Struct Biol* **163**, 258–269 (2008).
6. Mahrenholz, C. C., Abfalter, I. G., Bodenhofer, U., Volkmer, R. & Hochreiter, S. Complex networks govern coiled-coil oligomerization--predicting and profiling by means of a machine learning approach. *Mol Cell Proteomics* **10**, M110 004994 (2011).
7. Rackham, O. J. *et al.* The evolution and structure prediction of coiled coils across all genomes. *J Mol Biol* **403**, 480–493 (2010).
8. Knodler, L. A., Ibarra, J. A., Perez-Rueda, E., Yip, C. K. & Steele-Mortimer, O. Coiled-coil domains enhance the membrane association of Salmonella type III effectors. *Cell Microbiol* **13**, 1497–1517 (2011).
9. Delahay, R. M. & Frankel, G. Coiled-coil proteins associated with type III secretion systems: a versatile domain revisited. *Mol Microbiol* **45**, 905–916 (2002).
10. Hoiczyk, E., Roggenkamp, A., Reichenbecher, M., Lupas, A. & Heesemann, J. Structure and sequence analysis of Yersinia YadA and Moraxella UspAs reveal a novel class of adhesins. *EMBO J* **19**, 5989–5999 (2000).
11. Conners, R. *et al.* The Moraxella adhesin UspA1 binds to its human CEACAM1 receptor by a deformable trimeric coiled-coil. *EMBO J* **27**, 1779–1789 (2008).
12. Seifart Gomes, C. *et al.* Universal stress proteins are important for oxidative and acid stress resistance and growth of Listeria monocytogenes EGD-e in vitro and in vivo. *PLoS One* **6**, e24965 (2011).
13. Lupas, A. Coiled coils: new structures and new functions. *Trends Biochem Sci* **21**, 375–382 (1996).
14. Gruber, M., Soding, J. & Lupas, A. N. Comparative analysis of coiled-coil prediction methods. *J Struct Biol* **155**, 140–145 (2006).
15. Arhets, P., Olivo, J. C., Gounon, P., Sansonetti, P. & Guillen, N. Virulence and functions of myosin II are inhibited by overexpression of light meromyosin in Entamoeba histolytica. *Mol Biol Cell* **9**, 1537–1547 (1998).
16. Faust, D. M., Marquay Markiewicz, J., Danckaert, A., Soubigou, G. & Guillen, N. Human liver sinusoidal endothelial cells respond to interaction with Entamoeba histolytica by changes in morphology, integrin signalling and cell death. *Cell Microbiol* **13**, 1091–1106 (2011).
17. Solis, C. F., Santi-Rocca, J., Perdomo, D., Weber, C. & Guillen, N. Use of bacterially expressed dsRNA to downregulate Entamoeba histolytica gene expression. *PLoS One* **4**, e8424 (2009).
18. Kim, K. A. *et al.* NOX1 participates in ROS-dependent cell death of colon epithelial Caco2 cells induced by Entamoeba histolytica. *Microbes Infect* **13**, 1052–1061 (2011).
19. Padilla-Vaca, F., Ankri, S., Bracha, R., Koole, L. A. & Mirelman, D. Down regulation of Entamoeba histolytica virulence by monoxenic cultivation with Escherichia coli O55 is related to a decrease in expression of the light (35-kilodalton) subunit of the Gal/GalNAc lectin. *Infect Immun* **67**, 2096–2102 (1999).
20. Tovy, A. *et al.* Glucose starvation boosts Entamoeba histolytica virulence. *PLoS Negl Trop Dis* **5**, e1247 (2011).
21. Sahoo, N. *et al.* Calcium binding protein 1 of the protozoan parasite Entamoeba histolytica interacts with actin and is involved in cytoskeleton dynamics. *Journal of cell science* **117**, 3625–3634 (2004).
22. Lau, S. Y., Taneja, A. K. & Hodges, R. S. Synthesis of a model protein of defined secondary and quaternary structure. Effect of chain length on the stabilization and formation of two-stranded alpha-helical coiled-coils. *The Journal of biological chemistry* **259**, 13253–13261 (1984).
23. O'Shea, E. K., Lumb, K. J. & Kim, P. S. Peptide 'Velcro': design of a heterodimeric coiled coil. *Curr Biol* **3**, 658–667 (1993).
24. Grubisha, O. *et al.* DARPin-assisted crystallography of the CC2-LZ domain of NEMO reveals a coupling between dimerization and ubiquitin binding. *J Mol Biol* **395**, 89–104 (2010).
25. Wu, S. & Zhang, Y. LOMETS: a local meta-threading-server for protein structure prediction. *Nucleic Acids Res* **35**, 3375–3382 (2007).
26. Orozco, E., Guarneros, A. & Sanchez, T. Entamoeba histolytica. Phagocytosis as a virulence factor. *J Exp Med* **158**, 1511–1521 (1983).
27. Bailey, G. B., Gilmour, J. R. & McCoomer, N. E. Roles of target cell membrane carbohydrate and lipid in Entamoeba histolytica interaction with mammalian cells. *Infect Immun* **58**, 2389–2391 (1990).
28. Nachin, L., Nannmark, U. & Nystrom, T. Differential roles of the universal stress proteins of Escherichia coli in oxidative stress resistance, adhesion, and motility. *J Bacteriol* **187**, 6265–6272 (2005).
29. Tavares, P. *et al.* Roles of cell adhesion and cytoskeleton activity in Entamoeba histolytica pathogenesis: a delicate balance. *Infect Immun* **73**, 1771–1778 (2005).
30. Coudrier, E. *et al.* Myosin II and the Gal-GalNAc lectin play a crucial role in tissue invasion by Entamoeba histolytica. *Cell Microbiol* **7**, 19–27 (2005).
31. Mason, J. M. & Arndt, K. M. Coiled coil domains: stability, specificity, and biological implications. *Chembiochem* **5**, 170–176 (2004).
32. Peters, J., Baumeister, W. & Lupas, A. Hyperthermostable surface layer protein tetrabrachion from the archaebacterium Staphylothermus marinus: evidence for the presence of a right-handed coiled coil derived from the primary structure. *J Mol Biol* **257**, 1031–1041 (1996).
33. Diamond, L. S. Axenic cultivation of Entamoeba hitolytica. *Science* **134**, 336–337 (1961).
34. Hamann, L., Buss, H. & Tannich, E. Tetracycline-controlled gene expression in Entamoeba histolytica. *Molecular and biochemical parasitology* **84**, 83–91 (1997).
35. Bastida-Corcuera, F. D., Okumura, C. Y., Colocoussi, A. & Johnson, P. J. Trichomonas vaginalis lipophosphoglycan mutants have reduced adherence and cytotoxicity to human ectocervical cells. *Eukaryot Cell* **4**, 1951–1958 (2005).
36. Whitmore, L. & Wallace, B. A. DICHROWEB, an online server for protein secondary structure analyses from circular dichroism spectroscopic data. *Nucleic Acids Res* **32**, W668–673 (2004).
37. Whitmore, L. & Wallace, B. A. Protein secondary structure analyses from circular dichroism spectroscopy: methods and reference databases. *Biopolymers* **89**, 392–400 (2008).
38. Lees, J. G., Miles, A. J., Wien, F. & Wallace, B. A. A reference database for circular dichroism spectroscopy covering fold and secondary structure space. *Bioinformatics* **22**, 1955–1962 (2006).
39. Santoro, M. M. & Bolen, D. W. Unfolding free energy changes determined by the linear extrapolation method. 1. Unfolding of phenylmethanesulfonyl alpha-chymotrypsin using different denaturants. *Biochemistry* **27**, 8063–8068 (1988).

40. Swint, L. & Robertson, A. D. Thermodynamics of unfolding for turkey ovomucoid third domain: thermal and chemical denaturation. *Protein Sci* **2**, 2037–2049 (1993).

Acknowledgements

Author contributions

DP, BB, BR performed the experiments. DP, ARD performed bioinformatics analysis. DP, NG wrote the paper. NG, PE, ARD conceived the experiments.

Additional information

Supplementary information accompanies this paper at http://www.nature.com/scientificreports

Competing financial interests: The authors declare no competing financial interests.

How to cite this article: Perdomo, D. *et al*. The α-helical regions of KERP1 are important in *Entamoeba histolytica* adherence to human cells. *Sci. Rep.* **3**, 1171; DOI:10.1038/srep01171 (2013).